Valley photonic crystals

Jian-Wei Liu, Fu-Long Shi, Xin-Tao He, Guo-Jing Tang, Wen-Jie Chen, Xiao-Dong Chen & Jian-Wen Dong

Published online: 25 Apr 2021.

Submit your article to this journal ⤤

View related articles ⤤

View Crossmark data ⤤

Taylor & Francis
Taylor & Francis Group

Valley photonic crystals

Jian-Wei Liu[†], Fu-Long Shi[†], Xin-Tao He[†], Guo-Jing Tang ⓘ, Wen-Jie Chen, Xiao-Dong Chen ⓘ and Jian-Wen Dong ⓘ

School of Physics & State Key Laboratory of Optoelectronic Materials and Technologies, Sun Yat-sen University, Guangzhou China

ABSTRACT

Topological photonics is an emerging field that attracts enormous interest for its novel ways to engineer the flow of light. With the help of topological protection, the surface modes of topological photonic systems have intriguing properties, such as the unidirectional propagation, robust transmission against defects and disorders, which meet the rapidly growing demands for information processing. Valley photonic crystals, as one kind of topological photonic systems, not only support protected surface modes, but also are friendly to micro-nano fabrication. These advantages show that it has broad prospects in constructing high-performance photonic devices or even photonic integrated circuits. Here, we review the properties and development of valley photonic crystals. Firstly, the theory and structure are briefly introduced and then the discussion of robust transmission will be followed. Furthermore, prototypes of on-chip devices based on valley photonic crystals are reviewed. As a perspective in photonics, valley photonic crystal is expected to become a good platform to study nanophotonics and realize advancing integrated photonics devices.
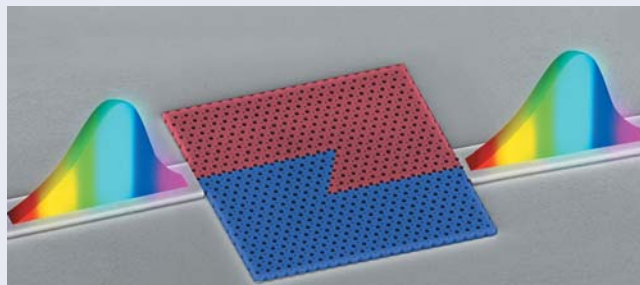
1. Introduction

Topology, which is a branch of mathematics, concerns with the invariant global properties under continuous deformation. In recent years, people have

CONTACT Jian-Wen Dong ✉ dongjwen@mail.sysu.edu.cn; Xiao-Dong Chen ✉ chenxd67@mail.sysu.edu.cn
School of Physics & State Key Laboratory of Optoelectronic Materials and Technologies, Sun Yat-sen University, Guangzhou 510275, China.
[†]These authors contributed equally to this work.

introduced topology into optical systems and found that defects and disorder can cause changes of local parameters but do not affect the global properties of topological photonic structures [1–5]. Therefore, topological photonic structures are stable and tolerant of micro-nano fabrication errors, and can be used for low-loss photonic information transmission. Different structures, such as metamaterials [6–9], coupled resonator optical waveguides [10–13], photonic crystals (PCs) [14–18], and helical waveguides [19–22], have been demonstrated as good platforms to achieve topological phenomena, and topological behaviors have been theoretically proposed and experimentally implemented in different photonic structures with various dimensions.

For the one-dimensional (1D) photonic systems, the topological property of the Su–Schrieffer–Heeger model is described by the Zak phase. As shown in Figure 1(a), the relationship between the Zak phase of bulk band of 1D
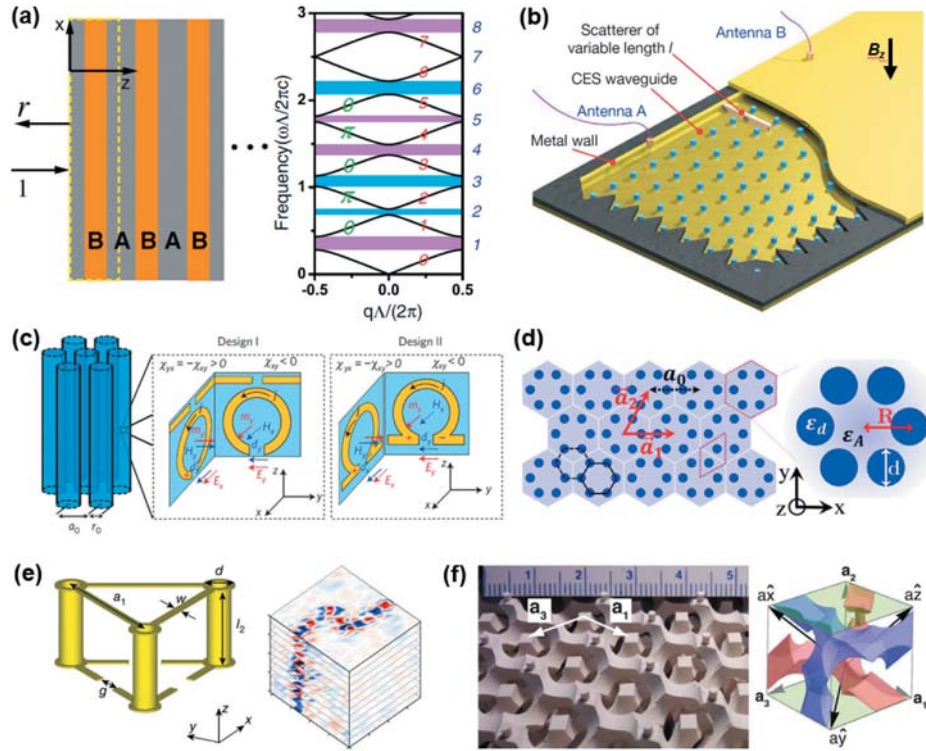

Figure 1. **Topological photonic crystals**. (a) A 1D dielectric PC and its band structure characterized by Zak phases [15]. (b) A 2D magneto-optical PC with broken time-reversal symmetry [16]. The external magnetic field is applied along the z direction. (c) A 2D metacrystal comprising a triangular lattice of spin-degenerate metamaterials and two possible microscopic structures [29]. (d) A 2D all-dielectric spin Hall PC with a hexagonal supercell instead of the rhombic unit cell [32]. (e) A 3D topological PC in which robust surface states were demonstrated [48]. (f) A 3D inversion symmetry-breaking double-gyroid PC whose band structure contains the Weyl point [18]. Figures reproduced from: (a) ref [15], Copyright 2014, American Physical Society; (b) ref [16], Copyright 2009, Nature Publishing Group; (c) ref [29], Copyright 2012, Nature Publishing Group; (d) ref [32], Copyright 2015, American Physical Society; (e) ref [48], Copyright 2019, Nature Publishing Group; (f) ref [18], Copyright 2015, American Association for the Advancement of Science.

PC and its surface impedance was revealed [15]. The interface where two 1D PCs with different Zak phases are placed side by side supports a confined mode. In addition to 1D PCs, topological behaviors in optical waveguide arrays [23], 1D metamaterials [6], and zigzag chain of plasmonic nanoparticles [24] have also been studied. In particular, because the zigzag chain structure is easy to be prepared, it has recently been used to realize topological lasing [25]. Two-dimensional (2D) topological photonic systems contain photonic quantum Hall system [16,26–28], photonic quantum spin Hall system [29–34], and photonic quantum valley Hall system [35–38]. As a seminal work, F. D. M. Haldane and S. Raghu first proposed the photonic quantum Hall effect in PCs by breaking the time-reversal symmetry [26]. To break the time-reversal symmetry, one can apply an external magnetic field to the magneto-optical material [16,28]. For example in Figure 1(b), a square lattice of magnetic PC was constructed and unidirectional robust edge states were measured [16]. Another way to break the time-reversal symmetry is to use time modulation to generate an effective magnetic field [39]. In addition, researchers proposed a photonic Floquet topological insulator [19], in which the periodicity along the propagation direction in the helical waveguides acts as 'time' modulation. Challenges in breaking time-reversal symmetry have motivated the search for time-reversal systems, thus the photonic quantum spin Hall system has been studied. Because of the natural difference between fermion (electron) and boson (photon), the key to realize photonic quantum spin Hall system is to form the pseudospins in photonic systems. Researchers have realized this in coupled resonator optical waveguides arrays [10,40], electromagnetic dual (or ε/μ matched) metamaterials [29–31,34,41], and dielectric PCs [32]. For example in Figure 1(c), researchers have proposed photonic topological insulators (PTIs) in electromagnetic dual photonic metacrystals [29]. In this metacrystal, modes with $E_z = H_z$ were defined as pseudospin-up and modes with $E_z = -H_z$ as pseudospin-down. On the other hand in Figure 1(d), photonic quantum spin Hall effect was also proposed [32] and later achieved [42–45] in honeycomb dielectric PCs. Two PCs with different spin Chern numbers were obtained by expanding and shrinking rods within the unit cell. Three-dimensional (3D) topological photonic structures can be divided into two categories, one is the 3D PTI and the other is 3D photonic topological semimetal. Examples of the structures of a 3D PTI and a 3D photonic topological semimetal are shown in Figure 1(e) and (f), respectively. The 3D PTIs can be seen as an extension of PTIs from 2D to 3D, which maintain a 3D photonic band gap separating two topological photonic bands. Various structures were proposed to realize 3D PTI [46–48] and the topological characteristics, such as Dirac-like surface states and robust surface propagation, have been experimentally demonstrated. Unlike the 3D PTIs, the 3D photonic topological semimetals have no 2D counterpart.

A typical manifestation of 3D photonic topological semimetals is the 0D Weyl degeneracy, also called the Weyl point. Similar to the 3D PTIs, surface states (called fermi arcs) are supported at the surface of 3D photonic semimetals and they connect the pairs of Weyl point [17,18]. In addition, multiple Weyl points [49], type-II Weyl points [20,50], ideal Weyl points [51], and Weyl points in synthetic systems [52] have been realized in PCs.

Compared with the 1D system, the 2D system has more parameters to be controlled, and compared with the 3D system, it is simpler to be fabricated. In particular, 2D topological PC is an advantageous topological photonic platform and is matched with the development of integrated optoelectronic devices. Recently, the valley binary degree of freedom has been introduced and photonic valley Hall effect has been realized in 2D PCs [35–38,53–57]. As photonic quantum valley Hall system only needs inversion symmetry breaking, the 2D valley photonic crystals (VPCs) can be easily designed with all-dielectric materials and combined with traditional processing techniques to prepare nanophotonic devices. Here, we review the properties and development of VPCs. Firstly, the theory and structures of VPCs are briefly introduced. Then the discussion of robust transmission will be followed, including experiments from microwave region to near-infrared (NIR) region. Furthermore, prototypes of on-chip devices designed with VPCs are discussed, including routing, resonator, and beam splitter. Also, some reconfigurable and active effects, which can be utilized to realized optical switch and lasing, are reviewed. Finally, the advantages and problems of VPCs will be mentioned.

2. Proposal and realization

The key to realize VPCs is breaking the inversion (mirror) symmetry to open the Dirac cone. Taking the honeycomb PC as an example, we briefly illustrate the relation between symmetry, band structure, and valley Chern number. As shown in Figure 2(a), when the inversion symmetry is preserved, the symmetry operations keeping the K (or K') point invariant are $M_K = \{E, 2C_3, 3\sigma_y\} = C_{3v}$. Around the K (or K') point, bands are linear and constitute a cone, i.e. the Dirac cone. When the inversion symmetry is broken by introducing perturbation on two different sublattices [Figure 2(b)], the symmetry of K point is reduced into C_3 symmetry whose symmetry operations are $\{E, 2C_3\}$. Due to the broken inversion symmetry, a resultant band gap is obtained and the frequency extremes of bands, i.e. valleys, are formed. As the time-reversal symmetry is preserved, the Berry curvatures satisfy $F(\mathbf{k}) = -F(-\mathbf{k})$ and the Chern number is zero. However, the Berry curvatures are locally nonzero at each valley and are opposite at K and K' valleys. Therefore, the VPC has a nonzero valley Chern number $C_v = C_K - C_{K'} = 2C_K$, which is calculated within half of the Brillouin zone around the valley. VPCs with opposite perturbations on two sublattices in Figure 2(b) and (c) have opposite valley
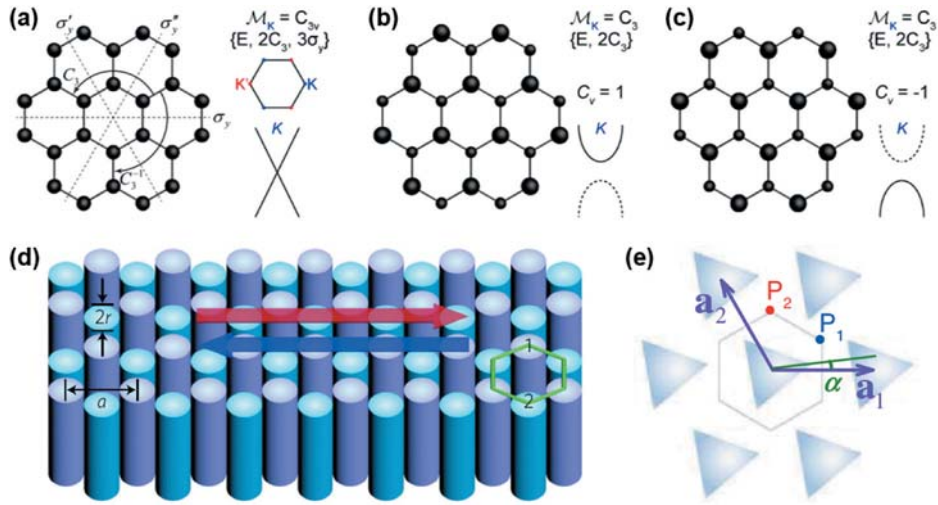
Figure 2. The relation between symmetry, band structure, and valley Chern number in valley crystals. (a) A 2D honeycomb PC with the symmetry operations of K and K' points at the corners of the Brillouin zone. The symmetry operations keeping K (or K') point invariant are M_K = {E, $2C_3$, $3\sigma_v$} = C_{3v}. The band structures around K (or K') valley are linear and constitute a cone, i.e. Dirac cone. (b, c) When the inversion symmetry is broken, the symmetry of K point reduces into C_3, which has symmetry operations of {E, $2C_3$}. A resultant band gap is obtained and frequency extremas of band structures, i.e. valleys, are formed. PCs with the opposite perturbation on two sublattices in (b) and (c) have opposite valley Chern numbers, which are quantized to be 1 and −1. (d) A honeycomb VPC whose inversion symmetry is broken by staggered bianisotropy in two rods [35]. (e) A triangular lattice structure with triangular atoms realizing valley sonic crystals [72]. Figures reproduced from: (d) ref [35], Copyright 2016, Nature Publishing Group; (e) ref [72], Copyright 2016, American Physical Society.

Chern numbers, which are quantized to be 1 and −1. At the domain wall between structures with distinct valley Chern number, there exist robust valley-dependent edge states against perturbations that do not cause inter-valley scattering. In condensed-matter physics, such kind of edge states is sometimes referred to as valley Hall kink states, which distinguish this kind of edge states from the conventional ones that exist at the periphery of a topological insulator [58]. The honeycomb PCs (or the photonic analog of graphene) have been studied [59–62], and recently the valley degree of freedom has been introduced [35–38,53–57,63–71]. Figure 2(d) shows a typical honeycomb VPC with broken inversion symmetry [35]. Note that another structure with triangular atoms as shown in Figure 2(e) breaks the mirror symmetry and valley sonic crystals were realized [72–74].

As the time-reversal symmetry is preserved and the requirement is the broken inversion symmetry, VPCs can be achieved in different structures. Tzuhsuan Ma and Gennady Shvets considered the 2D triangular PC [Figure 3 (a)] and studied its transverse electric (TE) modes [36]. The inversion symmetry was broken by using the triangular silicon rod in the unit cell. Then a complete band gap with nonzero valley Chern number was obtained
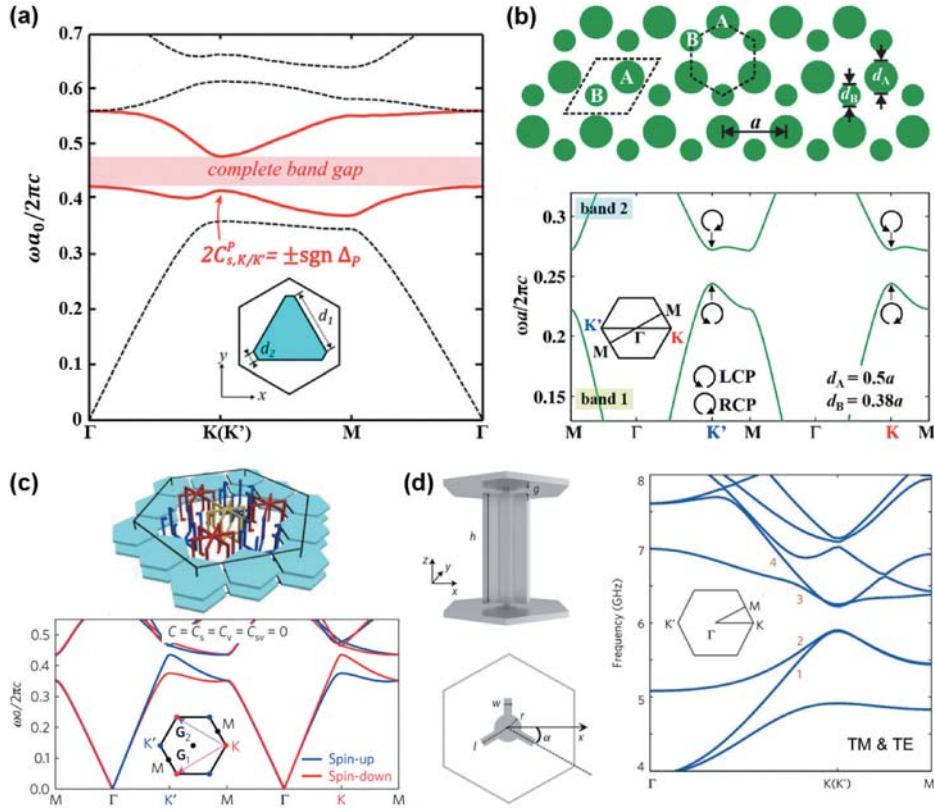
Figure 3. Valley photonic crystals. (a, b) VPCs with band structure consisting of one single polarization. For the triangular lattice of triangular silicon rods in (a), TE modes are considered [36]. While for the honeycomb lattice of circular dielectric rods in (b), TM modes are considered [37]. In both lattices, the Dirac cone is open and a complete band gap can be achieved. (c, d) VPCs with band structure consisting of dual polarization (spin-up and spin-down or TM and TE). (c) In the triangular lattice of ε/μ-matched metamaterials, dispersions of different spin states split in the frequency level due to the valley–spin coupling [35]. (d) In the triangular lattice of Y-shaped tripods between two parallel metallic plates, a band gap emerges near the K(K′) valleys for both TM/TE polarizations [38]. Figures reproduced from: (a) ref [36], Copyright 2016, Institute of Physics Publishing Group; (b) ref [37], Copyright 2017, American Physical Society; (c) ref [35], Copyright 2016, Nature Publishing Group; (d) ref [38], Copyright 2017, Nature Publishing Group.

between the second and third bands, which originally form the Dirac cone. The interface between two PCs with different symmetry-breaking geometries supports robust edge states. Topological protection against backscattering enables near-perfect out-coupling efficiency and reflection-free optical delays. Besides the TE modes, transverse magnetic (TM) modes of 2D VPCs have also been considered [37]. As shown in Figure 3(b), the inversion symmetry of PC was broken by changing the diameters of two cylinders in the unit cell. Different valleys states have different phase vortex, i.e. the K′ valley state has a left circular polarized (LCP) phase vortex while the K valley state has a right circular polarized (RCP) phase vortex. This valley-contrasting physics leads to

different transmission properties, such as unidirectional excitation of bulk states by a chiral source. In addition, valley photonics have also been studied in systems with both polarizations [35,38,53]. For example, an electromagnetic dual VPC was proposed in Figure 3(c) [35]. The metallic metamaterials were designed to satisfy the electromagnetic dual symmetry. To break the inversion symmetry, the bianisotropy tensors of different cylinders in the unit cell were reversed. This makes pseudospin bulk states split in the K' and K valleys, and results in the photonic valley Hall effect, i.e. different pseudospin bulk states propagate along opposite directions. The electromagnetic dual symmetry can also be achieved by the accidental degeneracy of TE and TM modes at the boundary of the Brillouin zone [29,31]. For example, an electromagnetic dual VPC consists of Y-shaped metallic rods sandwiched by two metal plates [38]. As shown in Figure 3(d), TE and TM modes are accidentally degenerate by tuning the structural parameters of metallic rods. When the inversion symmetry is broken, a complete band gap of both TE and TM modes is formed near the K and K' valleys.

Due to the simple structure and relieved material requirement, researchers soon realized VPCs in microwave frequency band [38,54,55,63,64,75]. They designed different structures and experimentally demonstrated the unidirectional emission, valley-locked beam splitting of bulk states, robust transport of edge states, and other phenomena. The first kind of proposed structures is the metallic parallel-plate waveguide with sandwiched periodic materials that simulates 2D structure. In this structure, rods in the middle layer are dielectric or metal arrays with broken inversion symmetry, and the upper and lower metal layers are regarded as perfect electric conductors. For example, by sandwiching Y-shaped metallic rods with two metallic plates, Gao et al. gave a microwave realization of VPC, showing the robust transmission and topologically protected refraction of the valley kink states [38]. To concretely introduce the experimental phenomena of VPCs, we take the PC shown in Figure 4(a) as an example. This PC is composed of a metallic parallel-plate waveguide filled with a triangular array of Y-shaped aluminum rods (top plate was removed) [55]. The K and K' valley bulk states have opposite chiral phase vortex. The chiral feature of the valley bulk states enables a selective excitation by a point-like chiral source [left panel of Figure 4(a)]. The measured E_z field excited by a clockwise phase delay source in Figure 4(b) displays two outgoing beams away from each boundary. By inspecting on the wavefronts of the outgoing beams, researchers concluded that the valley states at the K point are excited. Another structure to realized photonic valley Hall effect is the metal VPC without a top plate [63,64,76]. As an example, researchers placed the honeycomb lattice of metal rods on the metal plate and broke the inversion symmetry by adjusting the height of different pillars [Figure 4(c)]. They measured valley-chirality locked beam splitting [Figure 4(d)], in which the separated beams were constructed by different valleys and locked to the
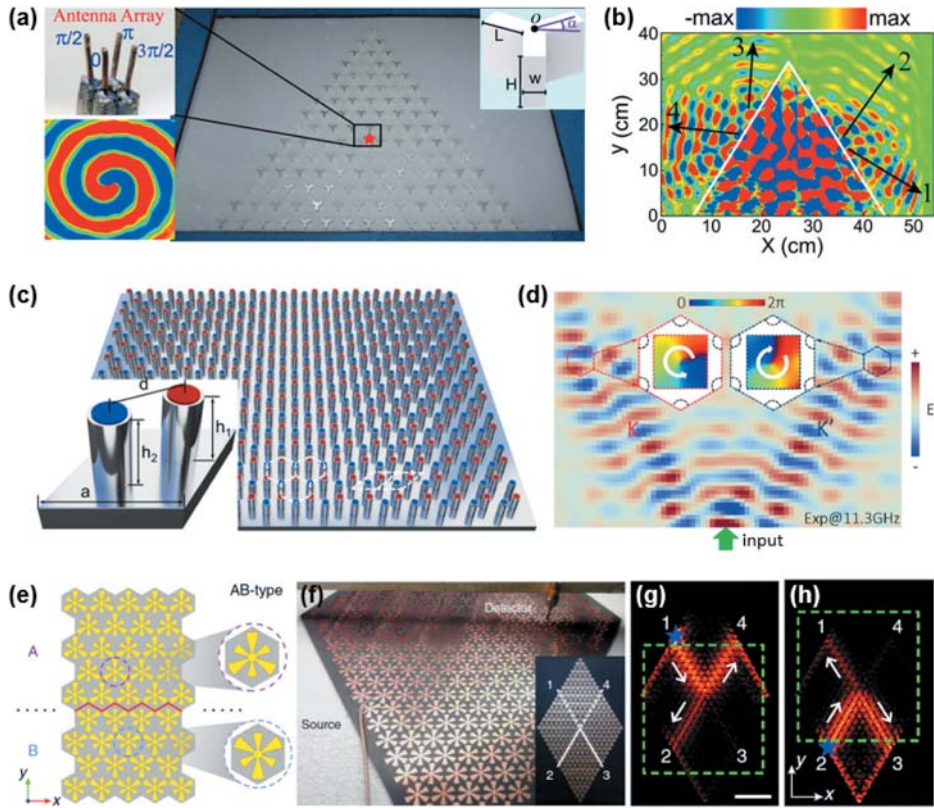
Figure 4. **Microwave experimental demonstration**. (a) VPC for the observation of bulk valley transport [55]. The upper-right inset shows the Y-shaped aluminum rod in unit cell, and the left inset shows the chiral source used to excite valley bulk states. (b) Measured E_z fields at the frequency of the lower valley state. (c) Surface-wave PC whose unit cell consists of two metallic rods with different heights standing on a metal surface [64]. (d) Measured valley-locked beam splitting. (e) A domain wall between two surface plasmon crystals with opposite valley Chern numbers [54]. (f) Experiment setup for topological transport of valley-polarized edge states. (g, h) Measured E_z fields of valley-polarized edge states when the input source is placed at different terminals. Figures reproduced from: (a, b) ref [55], Copyright 2017, American Institute of Physics Publishing Group; (c, d) ref [64], Copyright 2017, American Physical Society; (e-h) ref [54], Copyright 2017, Nature Publishing Group.

opposite chirality of the photonic valley pseudospin. Note that the metal VPC without a top plate can be structured on a deep-subwavelength scale, thus can confine light field tightly [63]. In addition, designer surface plasmon PCs, which can confine the waves in the vertical direction, are friendly to the direct observation of edge states. For example, a triangular designer surface plasmon VPC with metallic patterns on a dielectric substrate was studied [54]. The metallic pattern consists of an inner circle and six radial fans. The radius of the six fans can be changed to break the inversion symmetry. Robust edge states can be found at the domain wall between two inversion symmetric surface plasmon VPCs (patterns A and B), as shown in Figure 4(e). To selectively excite valley-polarized edge states, a rhombus-shaped beam splitter consisting of four domains was designed [Figure

4(f)]. E_z field were measured when the source is arranged at terminals 1 and 2, respectively. It can be observed that transports of edge states involving opposite valleys are suppressed (terminal 3 in Figure 4(g) and terminal 4 in Figure 4(h)). Thus, topological protection of the edge states at sharp corners is demonstrated.

Since VPCs have a variety of novel optical transmission properties, they can be used in the design of on-chip photonic devices. Recently, researchers have realized VPCs working at NIR or visible wavebands and detected their optical transmission properties. To combine with the traditional micro-nano processing technology, researchers use all-dielectric materials to fabricate VPCs. In 2018, researchers fabricated a 2D honeycomb array of laser-written evanescently coupled waveguides [65]. Armchair and zigzag domain walls were studied, and the zigzag one is shown in Figure 5(a). They presented the observed edge intensity ratio, which is the ratio of the light intensity along the domain wall to the light intensity in the bulk [Figure 5(b)]. The results (blue dots) prove that edge states can couple with the source waveguide near 1650 nm wavelength, and this work experimentally established the presence of valley Hall edge states at midgap. In addition, by utilizing honeycomb arrays, the light-valley interaction was studied and the generation of valley-contrasting vortices and vortex pairs was demonstrated [66,67]. On the other hand, PC slab is favorable of being integrated on chip, and it has become another platform for achieving VPCs. As PC slabs have 2D periodicity but a finite thickness, modes above the light cone will couple to the free space and radiate, but modes below the light cone behave like modes in 2D structure. Thus, researchers focus on the modes below the light cone. In 2019, researchers fabricated VPC slabs working at NIR frequency range [56,57]. The VPC slabs are arranged in a honeycomb lattice, and the inversion symmetry is broken by changing size of circle/triangular air holes of different sublattices. For example, the oblique view scanning electron microscope image of a fabricated silicon-on-insulator VPC slab is shown in Figure 5(c) [56]. Two VPCs, i.e. VPC1 and VPC2, are the inversion symmetry counterparts. They formed the interface that supports robust edge states. In Figure 5(d), three different shaped interfaces and the corresponding electromagnetic energy intensity patterns of edge states are shown. The electromagnetic energy intensities show that light can smoothly propagate around the corners without scattering. This intriguing property indicates the broadband robust transport due to the suppression of intervalley scattering. As another work in the same period, Shalaev et al. fabricated an on-chip VPC, which was composed of triangular air holes arranged in honeycomb lattice [57]. The schematic of the structure is shown in Figure 5(e). They used the grating to couple light into the system and built an experimental setup for transmittance measurement [left panel of Figure 5(f)]. The measured results of different shapes of domain wall are demonstrated at the right panel of Figure 5(f), showing the robustness of valley edge states of VPC waveguides. In 2020, researchers directly observed
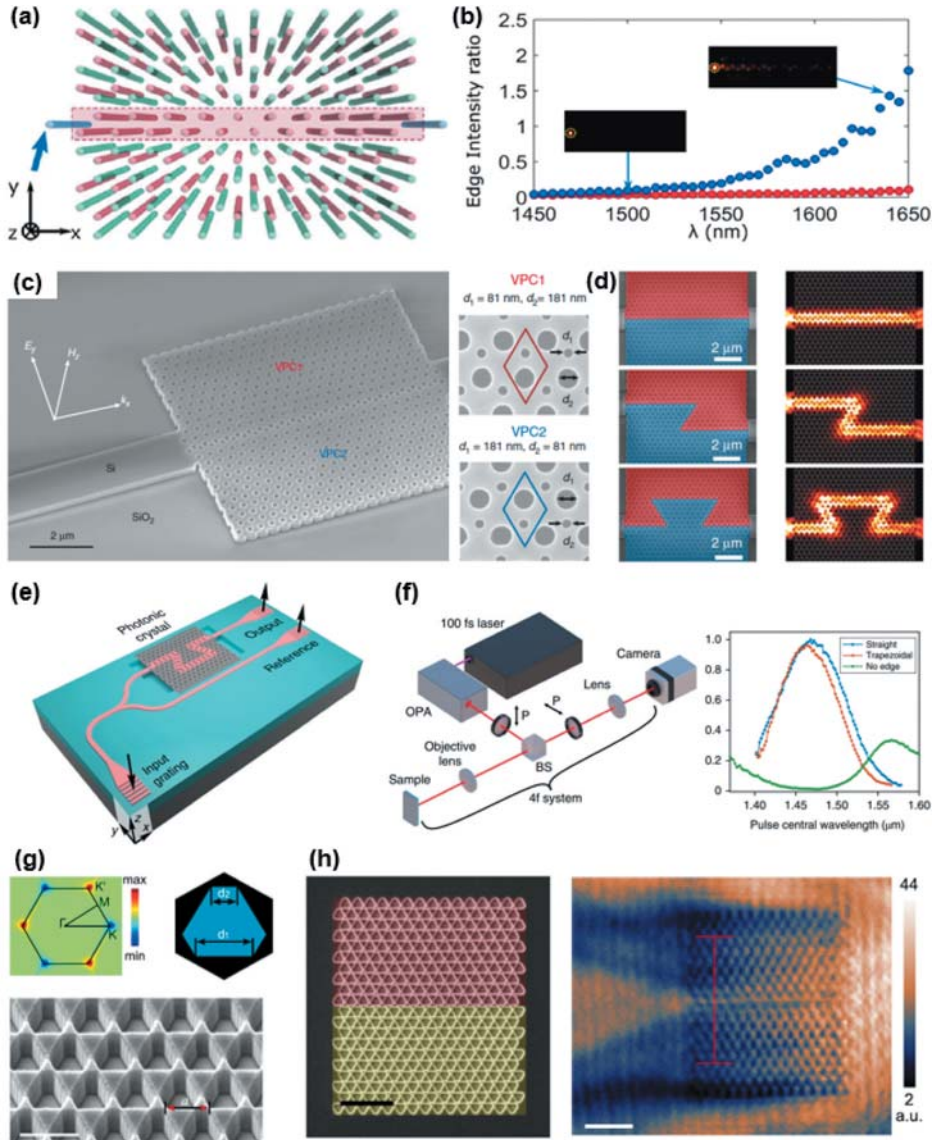
Figure 5. Near-infrared experimental demonstration. (a) Schematic diagram of inversion-symmetry-broken honeycomb lattices with zigzag domain walls [65]. Red and green wave-guides are characterized by different refractive index. (b) Measured edge intensity ratio when the midgap modes are excited. (c) Oblique view scanning electron microscope image of a fabricated silicon-on-insulator VPC slab [56]. VPC2 is the inversion partner of VPC1. (d) Fabricated samples and simulated electromagnetic energy intensities for the three different interfaces. (e) Schematic of the VPC structure. The photonic crystal is surrounded by air at the top and bottom. Light is coupled into (out of) the system by the input (output) grating [57]. (f) Left panel shows the experimental setup used for transmittance measurements while the right panel shows the corresponding measured results of different interfaces. (g) Design of the VPC slab for near-field mapping of edge modes [77]. (h) Scanning electron microscope image a VPC waveguide and near-field distribution of edge modes. Figures reproduced from: (a, b) ref [65], Copyright 2018, American Physical Society; (c, d) ref [56], Copyright 2019, Nature Publishing Group; (e, f) ref [57], Copyright 2019, Nature Publishing Group; (g, h) ref [77], Copyright 2020, American Institute of Physics Publishing Group.

the near-field profile of edge states in VPC slab working at NIR frequency range [77]. The VPC slab with triangular air-hole structure is shown in Figure 5(g), and TM-like modes were investigated. Two VPC slabs with opposite valley Chern numbers form the domain wall. The scanning electron microscope image and the near-field distribution of edge states are given in Figure 5(h). Light coupled into the bulk decay rapidly with the propagation distance, while the mode confined to the domain wall remains clearly visible.

3. Robust transmission

Robust transmission is one of the most significant properties of the VPC waveguides supporting valley-dependent modes. If there are no perturbations or defects that cause valley flipping in the systems, the light will be valley-locked and propagate unidirectionally. Such kinds of valley-dependent modes can be supported by the interface between VPCs with distinct valley Chern number, and it makes VPC a potential prospect in designing robust waveguide immune to shape bends. Figure 6(a) shows a simulated VPC waveguide whose transmitted edge mode locates at one valley [36]. The waveguide mode was excited by a launcher and coupled with a resonator. However, it is shown that the transmitted electromagnetic waves propagate to the right and the coupling with the resonator causes little energy backscattering. Moreover, the outgoing light from the VPC waveguide propagate upwards, suggesting that the refraction at VPC termination is also valley-locked. Such valley-locked refraction (or out-coupling) was observed by Gao et al. [38]. The refractions of edge states in VPC waveguides with a zigzag and armchair termination were studied. Figure 6(b) shows the microwave experimental observation of the refraction of TM-polarized kink states through a zigzag termination, suggesting that the VPC kink states can have a nearly perfect out-coupling.

To further explore the possibility of utilizing VPC waveguides for integrated photonic devices, experiments from microwave band [55,64,78,79] to terahertz (THz) band [69] or even NIR band [56,57,80,81] were demonstrated, verifying the robustness of VPC waveguides. In the microwave experiment, materials like dielectric rods and printed circuit boards are usually used. For example, Figure 6(c) shows a microwave experimental work from Chen et al. in 2019 [78]. In this work, they used printed circuit boards to construct the VPC system and designed a dual-band system. This dual-band system supports two valley kink states at different frequencies in one VPC waveguide. With the high transmissions for the frequencies in the band gap region [brown shaded rectangle in Figure 6(c)], kink states in straight waveguide and Z-shaped waveguide were proved to propagate robustly. In addition, the good performance of VPC waveguides was also seen in NIR region [80]. The detailed field pattern of edge modes of VPC-slab waveguide was measured with the help of the phase-resolved near-field optical microscopy [Figure 6
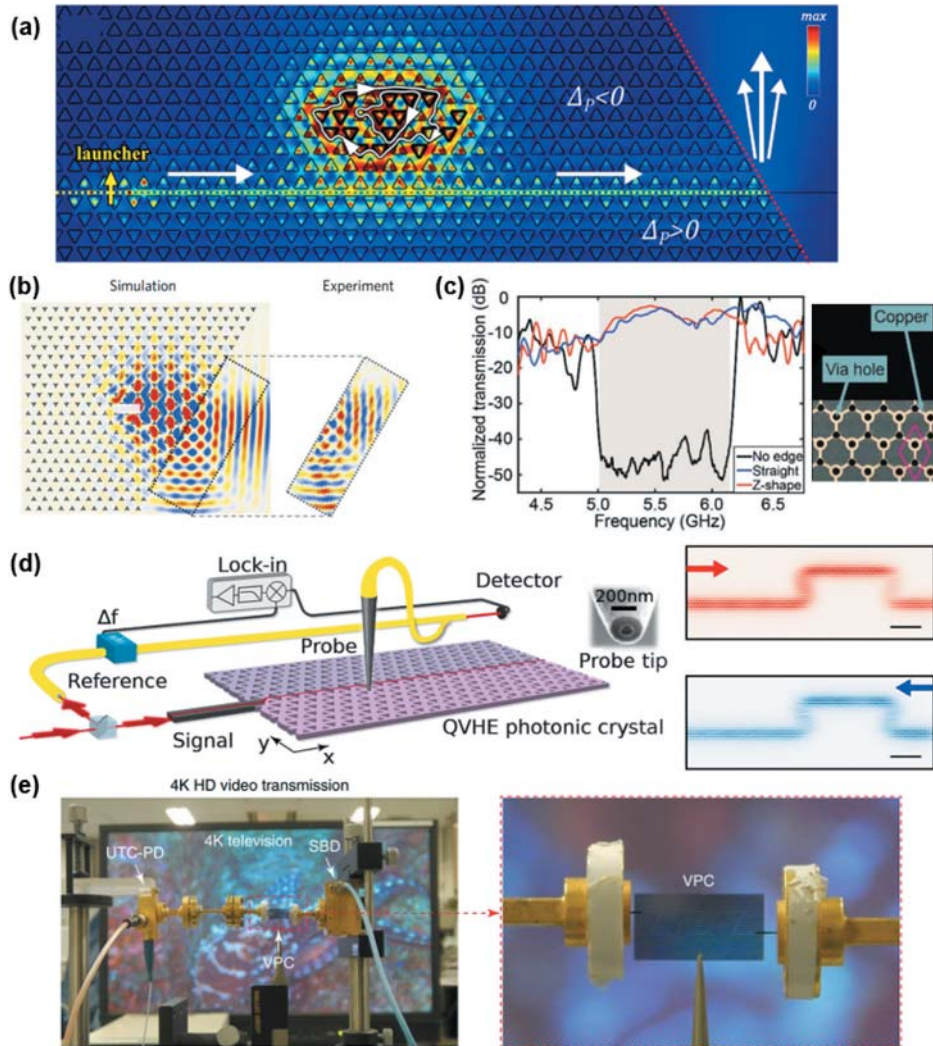
Figure 6. Robust and unidirectional propagation in VPC waveguides. (a) Simulated magnitude of H_z fields of edge states when the VPC waveguide is coupled with a whispering gallery-type resonator. The electromagnetic field is excited by a launcher and rightward propagation of edge states is confirmed [36]. (b) Refraction of TM-polarized kink states through the zigzag termination. The left panel is the simulated field pattern while the right panel is the measured one [38]. (c) Measured transmissions of kink states and the structure of the VPC sample based on printed circuit boards [78]. (d) Schematic of the near-field scanning optical microscope used to map the in-plane field distribution of the VPC edge modes. Measured real space amplitude maps of the modes propagating forward and backward are shown on the right [80]. (e) Experimental demonstration of uncompressed 4K high-definition video transmission with a VPC waveguide working on the terahertz frequency [69]. Figures reproduced from: (a) ref [36], Copyright 2016, Institute of Physics Publishing Group; (b) ref [38], Copyright 2017, Nature Publishing Group; (c) ref [78], Copyright 2019, WILEY-VCH; (d) ref [80], Copyright 2021, Nature Publishing Group; (e) ref [69], Copyright 2020, Nature Publishing Group.

(d)]. With a 200 nm subtle probe tip, the detailed sub-wavelength structure of the propagating modes was experimentally visualized. Lots of phenomena

indicate that VPC waveguide has a good performance in information processing. In 2020, Yang et al. constructed an on-chip VPC waveguide and used it to transfer the information of an uncompressed 4K video [69]. Figure 6(e) shows the experimental setup and the structure of the VPC. It can be seen that the 4K high-definition video is successfully transmitted in real-time through the VPC waveguide even with a twisted domain wall.

4. Prototypes of VPC devices

The unidirectional and robust transmission properties of VPC waveguides are suitable for the design of low-loss optical devices. With further research on VPCs, different kinds of prototypes of optical devices designed with VPC have been demonstrated, including router, cavity, beam filter, beam splitter, lasing, etc. We first review some of these prototypes of passive devices, then the reconfigurable and active devices.

4.1 Passive VPC devices

Router, one of the important components in integrated circuit, guides information to the desired direction. VPC waveguide is a potential platform to achieve this functionality based on its valley-locked propagating modes. Utilizing the correspondence between valley and chirality, a scheme of topological photonic routing was proposed [56]. The structure of such VPC routing sample is shown in Figure 7(a), including two VPC waveguides and a microdisk. When light incident from the strip silicon waveguides, a clockwise or anticlockwise phase vortex will be excited in the microdisk. Then, the light with different phase vortex will couple to different VPC waveguide in accordance with the chirality. Different from the above scheme, there are other routing structures based on valley-locked unidirectional propagation [79,82]. A scanning electron microscope image of a four-port routing working at telecom band is shown in Figure 7(b) [82]. Because the light propagation direction is dependent on the valley pseudospin, light injected into different channel will have different output. For example, when light is injected into channel 1, it will be routed into channels 2 and 4. Differently, the light injected into channel 2 will be routed into channels 1 and 3. The VPC router based on topological channel intersections was also proposed by Zhang et al. [79]. By utilizing the kink states at zigzag edge and armchair edge, they discussed a router with arbitrary geometry. One of the schemes is shown in Figure 7(c).

Mach–Zehnder interferometer (MZI) is one of the functional elements in on-chip photonic devices. It is broadly used in various integrated optical devices such as optical switches and sensors. The traditional silicon MZI has two typical difficulties. On one hand, the low propagation constant makes it a large waveguide length, typically several millimeters. On the other hand,
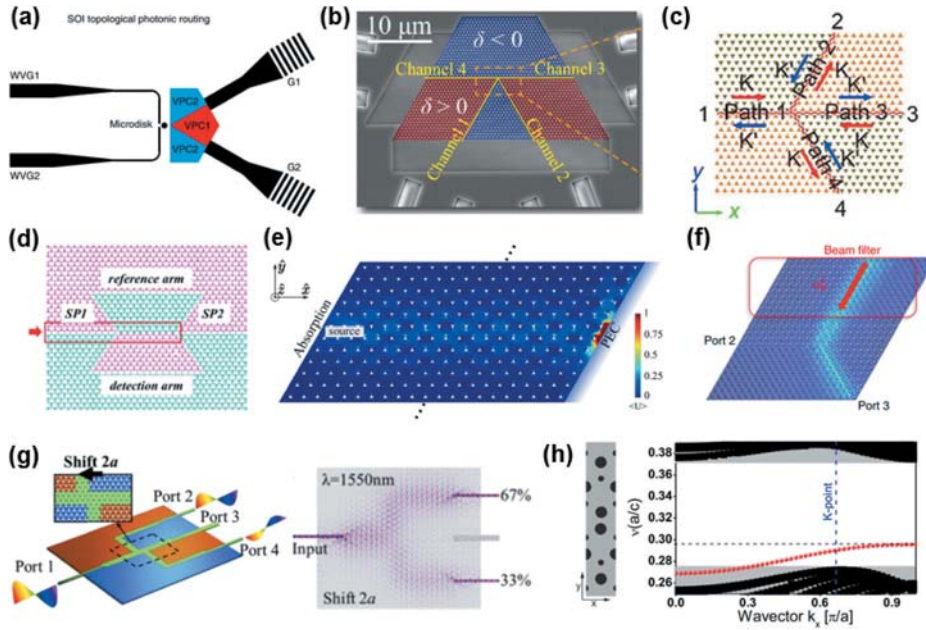
Figure 7. **Prototypes of passive photonic devices designed with VPC**. (a) Schematic of the topological photonic routing structure that consists of two VPC interfaces and a microdisk. Light come from WVG1 (WVG2) will excite an anticlockwise (clockwise) phase vortex in the microdisk and then couple to different valley chirality-locked modes in the VPC interfaces [56]. (b) Schematic of a four-channel VPC routing structure. Light injected into channel 1 is routed into channels 2 and 4, while light injected into channel 2 is routed into channels 1 and 3 [82]. (c) Schematic illustration of a topological channel intersection. The orange and green triangles represent the scatters with different structural parameters [79]. (d) Structure of the topologically protected Mach–Zehnder interferometer realized with VPC waveguide. Two types of VPC interface are utilized for the reference and detection arms [83]. (e) An optical cavity composed of a VPC waveguide and a mirror termination. The realization of the cavity is based on the near-conservation of the valley degree of freedom [84]. (f) A valley beam filter was realized by combining the valley degree and the spin degree of freedom [85]. The simulated transmission profile is shown, demonstrating that light with different valley polarization will be guided to different port. (g) The structure of a splitter based on VPC waveguide is depicted at the left panel while the corresponding energy distribution is shown at the right panel [89]. (h) The VPC structure and the corresponding edge dispersion of slow-light waveguide [90]. Figures reproduced from: (a) ref [56], Copyright 2019, Nature Publishing Group; (b) ref [82], Copyright 2019, WILEY-VCH; (c) ref [79], Copyright 2019, WILEY-VCH; (d) ref [83], Copyright 2020, Institute of Physics Publishing Group; (e) ref [84], Copyright 2020, American Physical Society; (f) ref [85], Copyright 2018, Nature Publishing Group; (g) ref [89], Copyright 2020, Optical Society of America; (h) ref [90], Copyright 2021, American Physical Society.

the backscattering loss caused by defects results in power drop of the device. To overcome these difficulties, a topologically protected MZI with VPC was proposed [83]. Figure 7(d) shows the structure of this topological MZI. The detection arm is filled with sample to be measured and the reference arm with air. By introducing the slow-light effects and with the help of robust transportation, the above two difficulties can be overcome.

Cavities have varieties of functionalities in practical optical devices. In 2020, Li et al. proposed a new kind of optical cavity based on the near-conservation of the valley degree of freedom (DOF) in VPC [84]. Valley-dependent modes will unidirectionally propagate when no valley flipping exists. Therefore, as shown in Figure 7(e), when putting a mirror at the termination of the VPC waveguide, the light will locate at the termination and not be reflected backward. Nevertheless, the effect of the localization is dependent on the shape of the termination. For example, the localization of a zigzag termination is much better than that of an armchair termination.

Combining valley DOF with other DOFs can realize much more functional devices. Various works were demonstrated to study the combination of valley DOF and pseudospin DOF [85,86] or the quantum anomalous Hall phases [87,88]. As demonstrated in Figure 7(f), a Y-junction of beam filter was constructed by combining the valley DOF and pseudospin DOF [85]. Utilizing these two DOFs, the light with different valley DOFs coming from the bus channel will be separated to different paths.

In addition, the performance of VPC can be improved by traditional optical optimization. For example, by modifying the interface of a VPC waveguide, a beam splitter with flexible splitting ratio can be achieved [89]. By inserting a few layers of Dirac-type lattice in the interface, the transmission performance of the edge modes becomes more adjustable. With the control of the relative space shift of the two output channels, the splitting ratio can be flexibly controlled, e.g. a 67:33 splitting ratio is demonstrated in Figure 7(g).

The slow-light property can be used for varieties of optical devices, including pulse delay and optical storage. However, the performance of the slow-light waveguide will be affected by the backscattering. Naturally, with the help of robust transmission, the VPC waveguide can be a good solution to this problem [90]. By using the VPC, a topologically protected slow-light waveguide was demonstrated, with its structure and dispersion shown in Figure 7 (h). To further quantify the robustness of such a VPC slow-light waveguide, researchers introduced a physical quantity called backscattering mean free path and quantitively compared the robustness of the VPC slow-light waveguides and conventional PC slow-light waveguides.

4.2 Reconfigurable and active VPC devices

With the novel transmission properties of VPC waveguides, a variety of high-performance optical components have been designed. However, the above structures or components operate in a fixed wavelength range and cannot be tunned actively. Tunability is an important and prospect property for many optical devices like modulators, switches, and optical buffers. A reconfigurable topological optical device will be essential in the integrated optical circuits. To overcome such a challenge, some studies on reconfigurable VPC systems were

proposed [71,91,92]. Most of the researches for dynamically tunning the VPC modes are based on tunning the permittivity or permeability of the VPC or the background materials. The usual ways to tune the permittivity of materials are light-beam pumping and electrical pumping. Utilizing the free carrier excitation of silicon, the refractive index can be modulated by a ultraviolet beam pumping [71]. Then, the change of refractive index results in the change of the band structure and also the position of band gap [Figure 8(a)]. With this dynamic control, an optical switch can be realized and the switching time is of the order of nanoseconds. In addition to using the pump beam to actively control the VPC systems, the external electric field can also be applied to control the VPCs by using electro-optic materials. For example, Figure 8(b) shows a VPC that is composed of TiO_2 and electro-optic material $BaTiO_3$ [91]. This PC rod slab is embedded in a SiO_2 layer and sandwiched by two gold films. By controlling the voltage between the two electrodes, namely the two gold films, the refractive index of the rods of $BaTiO_3$ is changed and
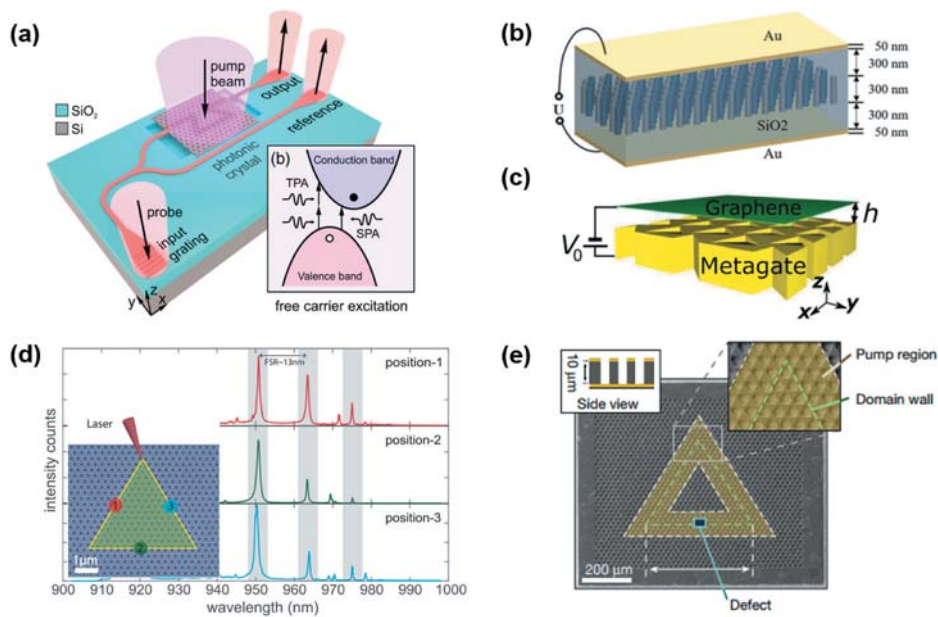

Figure 8. **Reconfigurable VPCs and lasing in VPCs**. (a) Schematic of the tunable VPC waveguide that is illuminated by an ultraviolet pump beam to control the refractive index of Si [71]. (b) Schematic of the tunable VPC configuration whose band structure can be controlled by the voltage applied between two gold films [91]. (c) Schematic of a graphene surface plasmon-based VPC. The metagate is placed within a few nanometers of graphene, and the band gap can be controlled by the voltage [92]. (d) The experimentally measured spectrum of the VPC resonator. The resonator modes are excited by a laser pump, and the inset shows the positions of the excitation and collection points [93]. (e) Structure of an electrically pumped VPC laser. The yellow area is the region pumped by electrical injection, and the green dashed line shows the domain wall of VPC [70].Figures reproduced from: (a) ref [71], Copyright 2019, Optical Society of America; (b) ref [91], Copyright 2018, American Physical Society; (c) ref [92], Copyright 2018, American Physical Society; (d) ref [93], reproduced under a Creative Commons Attribution 4.0 International License (http://creativecommons.org/licenses/by/4.0), Copyright 2020, American Physical Society; (e) ref [70], Copyright 2020, Nature Publishing Group.

consequently the strength of inversion symmetry is changed dynamically. As a result, the phase transition of the VPC is dynamically controlled. Utilizing the electrical-pumping method as well, there is also another reconfigurable system that combines VPC and graphene, whose structure is shown in Figure 8(c) [92]. By controlling the voltage and distance between graphene and the VPC, the graphene surface plasmons were dynamically controlled, and its topological phase transition was also actively controlled.

Active light source is a significant optical component in the integrated photonic circuits. They can be used in telecommunication, signal processing, imaging, and sensing. The robustness and chirality of valley kink states make valley Hall topological laser a promising device [68,70,93–95]. With the help of valley-locked propagating modes, a chiral topological resonator can be realized with VPC [93]. The schematic of a VPC resonator is shown in the inset of Figure 8(d). By using the quantum dots as the light source and pumping by laser, the resonating modes are excited. The positions of probing were set in three sides of the resonator, and Figure 8(d) shows the corresponding measured spectrums. The spectrums show that the VPC resonator supports three resonating modes and all have similar intensity distribution, which indicates the robustness of the VPC resonator. Moreover, by coupling the resonator with a straight waveguide, the chiral excitation of the VPC resonator can be demonstrated. Using the external laser source for optical pumping may not be friendly for compact integrated circuits. Instead, an electrically pumped quantum cascade laser designed with VPC may be a better solution [70]. As shown in Figure 8(e), layers of lattice on each sides of the domain wall of VPC are covered with gold as the electrodes, which are used to electrically pump the VPC. For the VPC waveguide is immune to defects and impurities, such VPC laser support high-efficiency resonant modes, ignoring the existence of shape corners and defects.

5. Summary and outlook

Over the past decade, technologies of information processing and inter-connecting have upgraded for generations. Realizing highly efficient and compact optical devices with lossless light transmission has become a rapidly growing demand. However, traditional optical devices, such as waveguides and resonators, suffer from losses caused by backscattering. Despite its infancy, topological photonics may be a new but potential mothed to design low-loss optical devices because of the robust transmission with immunity to defects and impurities endowed by topology.

As an important branch of topological photonics, VPCs not only have the advantages of robust transmission but also are friendly to micro-nano fabrication technology, which is suitable for designing compact on-chip optical devices. A large number of successful experiments from microwave band to NIR band have verified the robustness of VPC waveguides and

demonstrated the potential of using VPC to design optical devices. Furthermore, a variety of prototypes of on-chip optical devices have been successfully realized with VPCs, including router, laser, resonator, beam splitter, slow-light waveguide, etc. In addition, some kinds of reconfigurable or active devices have also been realized, which further enriches the functionality of VPC devices. Moreover, chiral light–matter interaction based on polarization-momentum locking of evanescent fields in nanophotonics is important and can be used to realize various functionalities. For example, it can be utilized to control the directionality of spontaneous emission and modify photon-mediated interactions between quantum emitters. With the help of the robustness of valley kink states, VPC waveguides may be a potential choice to realize the chiral topological waveguide coupled with quantum dots [93,96,97]. Besides PCs, many researches have demonstrated to study the spin–orbit coupling between 2D materials in valleytronics and optical structures, which is also a potential platform for precise on-chip information processing [98–101].

Though the VPC systems have obtained success in realizing lossless optical devices, there still exist challenges. The out-of-plane radiation of a VPC slab is one of the critical challenges. When light propagates in a VPC slab, the in-plane propagation of valley edge states is robust and protected by topology and the out-of-plane radiation is suppressed by index guiding, i.e. dispersion of the valley kink states is below the light cone. Nevertheless, when the valley kink states encounter scatters like shape bends (which are structures with finite sizes), the coupling between the valley states and the background (e.g. air) cannot be zero due to the breakdown of the conservation of wave vector. Although the radiation loss (along the out-of-plane direction) is small, it should be carefully checked for VPC devices designing for nanophotonics. On the other hand, when using VPC to design optical devices, the performance indexes of the VPC devices have to be considered and compared with that of the traditional optical devices. So far, some of the VPC devices have inferior performance indexes compared to their topological trivial counterparts. These are the challenges for designing VPC integrated photonic devices, but also the development directions.

ORCID

Guo-Jing Tang http://orcid.org/0000-0003-2379-554X
Xiao-Dong Chen http://orcid.org/0000-0001-8698-0609
Jian-Wen Dong http://orcid.org/0000-0003-2379-554X

References

[1] Ozawa T, Price HM, Amo A, et al. Topological photonics. Rev Mod Phys. 2019;91:015006.
[2] Lu L, Joannopoulos JD, Soljačić M. Topological photonics. Nat Photonics. 2014;8:821–829.
[3] Khanikaev AB, Shvets G. Two-dimensional topological photonics. Nat Photonics. 2017;11:763–773.
[4] Xie B-Y, Wang H-F, Zhu X-Y, et al. Photonics meets topology. Opt Express. 2018;26:24531.
[5] Iwamoto S, Ota Y, Arakawa Y. Recent progress in topological waveguides and nanocavities in a semiconductor photonic crystal platform. Opt Mater Express. 2021;11:319–337.
[6] Tan W, Sun Y, Chen H, et al. Photonic simulation of topological excitations in metamaterials. Sci Rep. 2014;4:3842.
[7] Gao W, Lawrence M, Yang B, et al. Topological photonic phase in chiral hyperbolic metamaterials. Phys Rev Lett. 2015;114:037402.
[8] Xiao M, Lin Q, Fan S. Hyperbolic weyl point in reciprocal chiral metamaterials. Phys Rev Lett. 2016;117:057401.
[9] Slobozhanyuk AP, Khanikaev AB, Filonov DS, et al. Experimental demonstration of topological effects in bianisotropic metamaterials. Sci Rep. 2016;6:22270.
[10] Hafezi M, Demler EA, Lukin MD, et al. Robust optical delay lines with topological protection. Nat Phys. 2011;7:907–912.
[11] Hafezi M, Mittal S, Fan J, et al. Imaging topological edge states in silicon photonics. Nat Photonics. 2013;7:1001–1005.
[12] Yin C, Chen Y, Jiang X, et al. Realizing topological edge states in a silicon nitride microring-based photonic integrated circuit. Opt Lett. 2016;41:4791.
[13] Liang GQ, Chong YD. Optical resonator analog of a two-dimensional topological insulator. Phys Rev Lett. 2013;110:203904.
[14] Poshakinskiy AV, Poddubny AN, Pilozzi L, et al. Radiative topological states in resonant photonic crystals. Phys Rev Lett. 2014;112:107403.
[15] Xiao M, Zhang ZQ, Chan CT. Surface impedance and bulk band geometric phases in one-dimensional systems. Phys Rev X. 2014;4:021017.
[16] Wang Z, Chong Y, Joannopoulos JD, et al. Observation of unidirectional backscattering-immune topological electromagnetic states. Nature. 2009;461:772–775.
[17] Lu L, Fu L, Joannopoulos JD, et al. Weyl points and line nodes in gyroid photonic crystal. Nat Photonics. 2013;7:294–299.

[18] Lu L, Wang Z, Ye D, et al. Experimental observation of Weyl points. Science. 2015;349:622–624.

[19] Rechtsman MC, Zeuner JM, Plotnik Y, et al. Photonic Floquet topological insulators. Nature. 2013;496:196–200.

[20] Noh J, Huang S, Leykam D, et al. Experimental observation of optical Weyl points and Fermi arc-like surface states. Nat Phys. 2017;13:611–617.

[21] Zhang W, Chen X, Ye F. Plasmonic topological insulators for topological nanophotonics. Opt Lett. 2017;42:4063–4066.

[22] Stutzer S, Plotnik Y, Lumer Y, et al. Photonic topological Anderson insulators. Nature. 2018;560:461–465.

[23] Blanco-Redondo A, Andonegui I, Collins MJ, et al. Topological optical waveguiding in silicon and the transition between topological and trivial defect states. Phys Rev Lett. 2016;116:163901.

[24] Poddubny A, Miroshnichenko A, Slobozhanyuk A, et al. Topological majorana states in zigzag chains of plasmonic nanoparticles. ACS Photonics. 2014;1:101–105.

[25] St-Jean P, Goblot V, Galopin E, et al. Lasing in topological edge states of a one-dimensional lattice. Nat Photonics. 2017;11:651–656.

[26] Haldane F, Raghu S. Possible realization of directional optical waveguides in photonic crystals with broken time-reversal symmetry. Phys Rev Lett. 2008;100:013904.

[27] Wang Z, Chong Y, Joannopoulos J, et al. Reflection-free one-way edge modes in a gyromagnetic photonic crystal. Phys Rev Lett. 2008;100:013905.

[28] Poo Y, Wu R-X, Lin Z, et al. Experimental realization of self-guiding unidirectional electromagnetic edge states. Phys Rev Lett. 2011;106:093903.

[29] Khanikaev AB, Mousavi SH, Tse W-K, et al. Photonic topological insulators. Nat Mater. 2013;12:233–239.

[30] Chen W-J, Jiang S-J, Chen X-D, et al. Experimental realization of photonic topological insulator in a uniaxial metacrystal waveguide. Nat Commun. 2014;5:5782.

[31] Ma T, Khanikaev AB, Mousavi SH, et al. Guiding electromagnetic waves around sharp corners: topologically protected photonic transport in metawaveguides. Phys Rev Lett. 2015;114:127401.

[32] Wu L-H, Hu X. Scheme for achieving a topological photonic crystal by using dielectric material. Phys Rev Lett. 2015;114:223901.

[33] Cheng X, Jouvaud C, Ni X, et al. Robust reconfigurable electromagnetic pathways within a photonic topological insulator. Nat Mater. 2016;15:542–548.

[34] He C, Sun X-C, Liu X-P, et al. Photonic topological insulator with broken time-reversal symmetry. Proc Nat Acad Sci. 2016;113:4924–4928.

[35] Dong J-W, Chen X-D, Zhu H, et al. Valley photonic crystals for control of spin and topology. Nat Mater. 2016;16:298–302.

[36] Ma T, Shvets G. All-si valley-Hall photonic topological insulator. New J Phys. 2016;18:025012.

[37] Chen X-D, Zhao F-L, Chen M, et al. Valley-contrasting physics in all-dielectric photonic crystals: orbital angular momentum and topological propagation. Phys Rev B. 2017;96:020202(R).

[38] Gao F, Xue H, Yang Z, et al. Topologically protected refraction of robust kink states in valley photonic crystals. Nat Phys. 2017;14:140–144.

[39] Fang K, Yu Z, Fan S. Realizing effective magnetic field for photons by controlling the phase of dynamic modulation. Nat Photonics. 2012;6:782–787.

[40] Gao F, Gao Z, Shi X, et al. Probing topological protection using a designer surface plasmon structure. Nat Commun. 2016;7:11619.

[41] Chen X-D, Deng W-M, Zhao F-L, et al. Accidental double dirac cones and robust edge states in topological anisotropic photonic crystals. Laser Photonics Rev. 2018;12:1800073.

[42] Yang Y, Xu YF, Xu T, et al. Visualization of a unidirectional electromagnetic waveguide using topological photonic crystals made of dielectric materials. Phys Rev Lett. 2018;120:217401.

[43] Yang Y, Hang ZH. Topological whispering gallery modes in two-dimensional photonic crystal cavities. Opt Express. 2018;26:21235–21241.

[44] Gorlach MA, Ni X, Smirnova DA, et al. Far-field probing of leaky topological states in all-dielectric metasurfaces. Nat Commun. 2018;9:909.

[45] Peng S, Schilder NJ, Ni X, et al. Probing the band structure of topological silicon photonic lattices in the visible spectrum. Phys Rev Lett. 2019;122:117401.

[46] Lu L, Fang C, Fu L, et al. Symmetry-protected topological photonic crystal in three dimensions. Nat Phys. 2016;12:337–340.

[47] Slobozhanyuk A, Mousavi SH, Ni X, et al. Three-dimensional all-dielectric photonic topological insulators. Nat Photonics. 2017;11:130–136.

[48] Yang Y, Gao Z, Xue H, et al. Realization of a three-dimensional photonic topological insulator. Nature. 2019;565:622–626.

[49] Chen W-J, Xiao M, Chan CT. Photonic crystals possessing multiple Weyl points and the experimental observation of robust surface states. Nat Commun. 2016;7:13038.

[50] Gao W, Yang B, Lawrence M, et al. Photonic Weyl degeneracies in magnetized plasma. Nat Commun. 2016;7:12435.

[51] Yang B, Guo Q, Tremain B, et al. Ideal Weyl points and helicoid surface states in artificial photonic crystal structures. Science. 2018;359:1013–1016.

[52] Wang Q, Xiao M, Liu H, et al. Optical interface states protected by synthetic weyl points. Phys Rev X. 2017;7:031032.

[53] Ma T, Shvets G. Scattering-free edge states between heterogeneous photonic topological insulators. Phys Rev B. 2017;95:165102.

[54] Wu X, Meng Y, Tian J, et al. Direct observation of valley-polarized topological edge states in designer surface plasmon crystals. Nat Commun. 2017;8:1304.

[55] Ye L, Yang Y, Hong Hang Z, et al. Observation of valley-selective microwave transport in photonic crystals. Appl Phys Lett. 2017;111:251107.

[56] He X-T, Liang E-T, Yuan -J-J, et al. A silicon-on-insulator slab for topological valley transport. Nat Commun. 2019;10:872.

[57] Shalaev MI, Walasik W, Tsukernik A, et al. Robust topologically protected transport in photonic crystals at telecommunication wavelengths. Nature Nanotechnology. 2019;14:31–34.

[58] Jung J, Zhang F, Qiao Z, et al. Valley-Hall kink and edge states in multilayer graphene. Phys Rev B. 2011;84:075418.

[59] Ochiai T, Onoda M. Photonic analog of graphene model and its extension: dirac cone, symmetry, and edge states. Phys Rev B. 2009;80:155103.

[60] Ochiai T. Photonic realization of the (2+1)-dimensional parity anomaly. Phys Rev B. 2012;86:075152.

[61] Deng F, Sun Y, Wang X, et al. Observation of valley-dependent beams in photonic graphene. Opt Express. 2014;22:23605–23613.

[62] Deng F, Li Y, Sun Y, et al. Valley-dependent beams controlled by pseudomagnetic field in distorted photonic graphene. Opt Lett. 2015;40:3380–3383.

[63] Yves S, Berthelot T, Lerosey G, et al. Locally polarized wave propagation through crystalline metamaterials. Phys Rev B. 2020;101:035127.

[64] Gao Z, Yang Z, Gao F, et al. Valley surface-wave photonic crystal and its bulk/edge transport. Phys Rev B. 2017;96:201402(R).

[65] Noh J, Huang S, Chen KP, et al. Observation of photonic topological valley hall edge states. Phys Rev Lett. 2018;120:063902.

[66] Song D, Paltoglou V, Liu S, et al. Unveiling pseudospin and angular momentum in photonic graphene. Nat Commun. 2015;6:6272.

[67] Song D, Leykam D, Su J, et al. Valley vortex states and degeneracy lifting via photonic higher-band excitation. Phys Rev Lett. 2019;122:123903.

[68] Smirnova D, Tripathi A, Kruk S, et al. Room-temperature lasing from nanophotonic topological cavities. Light Sci Appl. 2020;9:127.

[69] Yang Y, Yamagami Y, Yu X, et al. Terahertz topological photonics for on-chip communication. Nat Photonics. 2020;14:446–451.

[70] Zeng Y, Chattopadhyay U, Zhu B, et al. "Electrically pumped topological laser with valley edge modes. Nature. 2020;578:246–250.

[71] Shalaev MI, Walasik W, Litchinitser NM. Optically tunable topological photonic crystal. Optica. 2019;6:839–844.

[72] Lu J, Qiu C, Ke M, et al. Valley vortex states in sonic crystals. Phys Rev Lett. 2016;116:093901.

[73] Ye L, Qiu C, Lu J, et al. Observation of acoustic valley vortex states and valley-chirality locked beam splitting. Phys Rev B. 2017;95:174106.

[74] Wang M, Zhou W, Bi L, et al. Valley-locked waveguide transport in acoustic heterostructures. Nat Commun. 2020;11:3000.

[75] Chen X-D, Shi F-L, Liu H, et al. Tunable electromagnetic flow control in valley photonic crystal waveguides. Phys Rev Appl. 2018;10: 044002.

[76] Yves S, Fleury R, Berthelot T, et al. Crystalline metamaterials for topological properties at subwavelength scales. Nat Commun. 2017;8:16023.

[77] Dubrovkin AM, Chattopadhyay U, Qiang B, et al. Near-field mapping of the edge mode of a topological valley slab waveguide at λ=1.55μm. Appl Phys Lett. 2020;116:191105.

[78] Chen Q, Zhang L, He M, et al. Valley-Hall photonic topological insulators with dual-band kink states. Adv Opt Mater. 2019;7:1900036.

[79] Zhang L, Yang Y, He M, et al. Valley kink states and topological channel intersections in substrate-integrated photonic circuitry. Laser Photonics Rev. 2019;1900159. DOI:10.1002/lpor.201900159

[80] Arora S, Bauer T, Barczyk R, et al. Direct quantification of topological protection in symmetry-protected photonic edge states at telecom wavelengths. Light Sci Appl. 2021;10:9.

[81] Collins MJ, Zhang F, Bojko R, et al. Integrated optical Dirac physics via inversion symmetry breaking. Phys Rev A. 2016;94:063827.

[82] Ma J, Xi X, Sun X. Topological photonic integrated circuits based on valley kink states. Laser Photonics Rev. 2019;13:1900087.

[83] Yang P, Jiang P, Guo X, et al. Topologically protected Mach–Zehnder interferometer. J Opt. 2020;22:105001.

[84] Li Y, Yu Y, Liu F, et al. Topology-controlled photonic cavity based on the near-conservation of the valley degree of freedom. Phys Rev Lett. 2020;125:213902.

[85] Kang Y, Ni X, Cheng X, et al. Pseudo-spin-valley coupled edge states in a photonic topological insulator. Nat Commun. 2018;9:3029.

[86] Ni X, Purtseladze D, Smirnova DA, et al. Spin- and valley-polarized one-way Klein tunneling in photonic topological insulators. Sci Adv. 2018;4:8802.

[87] Lu J-C, Chen X-D, Deng W-M, et al. One-way propagation of bulk states and robust edge states in photonic crystals with broken inversion and time-reversal symmetries. J Opt. 2018;20:075103.

[88] Chan H-C, Guo G-Y. Tuning topological phase transitions in hexagonal photonic lattices made of triangular rods. Phys Rev B. 2018;97:045422.

[89] He L, Ji HY, Wang YJ, et al. Topologically protected beam splitters and logic gates based on two-dimensional silicon photonic crystal slabs. Opt Express. 2020;28:34015–34023.

[90] Arregui G, Gomis-Bresco J, Sotomayor-Torres CM, et al. Quantifying the robustness of topological slow light. Phys Rev Lett. 2021;126:027403.

[91] Wu Y, Hu X, Gong Q. Reconfigurable topological states in valley photonic crystals. Phys Rev Mater. 2018;2:122201.

[92] Jung M, Fan Z, Shvets G. Midinfrared plasmonic valleytronics in metagate-tuned graphene. Phys Rev Lett. 2018;121:086807.

[93] Barik S, Karasahin A, Mittal S, et al. Chiral quantum optics using a topological resonator. Phys Rev B. 2020;101:205303.

[94] Zhong H, Li Y, Song D, et al. Topological valley hall edge state lasing. Laser Photonics Rev. 2020;14:2000001.

[95] Gong Y, Wong S, Bennett AJ, et al. Topological INSULATOR LASER USING VALLEY-HALL PHOTONIC Crystals. ACS Photonics. 2020;7:2089–2097.

[96] Foster A, Jalali Mehrabad M, Dost R, et al. Chiral topological photonics with an embedded quantum emitter. Optica. 1690-1696;7:2020.

[97] Chen Y, He X-T, Cheng Y-J, et al., "Topologically protected valley-dependent quantum photonic circuits", arXiv2103.06686 (2021).

[98] Gong S-H, Alpeggiani F, Sciacca B, et al. Nanoscale chiral valley-photon interface through optical spin-orbit coupling. Science. 2018;359:443–447.

[99] Kamiya Y, Ge L, Hong T, et al. The nature of spin excitations in the one-third magnetization plateau phase of Ba3CoSb2O9. Nat Commun. 2018;9:2666.

[100] Sun L, Wang C-Y, Krasnok A, et al. Separation of valley excitons in a MoS2 monolayer using a subwavelength asymmetric groove array. Nat Photonics. 2019;13:180–184.

[101] Wang J, Li H, Ma Y, et al. Routing valley exciton emission of a WS2 monolayer via delocalized Bloch modes of in-plane inversion-symmetry-broken photonic crystal slabs. Light Sci Appl. 2020;9:148.